



Development of a dissolved oxygen sensor using tris(bipyridyl) ruthenium (II) complexes entrapped in highly siliceous zeolites

Pramatha Payra, Prabir K. Dutta *

Department of Chemistry, The Ohio State University, 120 West 18th Avenue, Columbus, OH 43210, USA

Received 25 April 2003; accepted 28 June 2003

Abstract

Defect-free highly siliceous zeolites were prepared by dealumination of zeolite Y using silicon tetrachloride. Tris(bipyridyl) ruthenium (II) complex, $[\text{Ru}(\text{bpy})_3]^{2+}$, was synthesized inside the supercages of the highly siliceous faujasitic zeolites using neutral $\text{Ru}(\text{bpy})\text{Cl}_3$ as the starting material. The conventional procedure using ion-exchange of hexammine ruthenium could not be used because of the lack of ion-exchange sites in the siliceous zeolites. The emission quenching of intrazeolitic $\text{Ru}(\text{bpy})_3^{2+}$ by oxygen dissolved in water was studied. Dealumination of the zeolitic framework leads to a hydrophobic environment that promotes oxygen transfer from water to the zeolite. Transparent zeolite-dispersed siloxane films were prepared and examined as sensors for dissolved oxygen.

© 2003 Elsevier Inc. All rights reserved.

Keywords: Siliceous zeolites; Oxygen sensor; Tris(bipyridyl) ruthenium (II)

1. Introduction

Oxygen analysis is important in determining the suitability of water for living organisms (biological oxygen demand), blood gas analysis, pressure sensitive paints, in vivo analysis, and in combustion monitoring [1]. Optical oxygen sensors offer advantages over electrochemical devices, including faster response, lack of analyte consumption and absence of electrical connections. The change in luminescence (or lifetime) of a sensitizer by energy transfer to oxygen is the basis of measurement for

optical oxygen sensors, with commonly used sensitizers being Ru(II) α -diimine complexes and porphyrins [1b,2].

A support matrix that can anchor the sensitizer as well as provide rapid permeation of oxygen, with minimal interferences and long-term stability is necessary. Siloxanes [3], due to their high permeability to oxygen, low glass-transition temperature and benign physiological response, various polymers [4] (polymethylmethacrylate, polyvinyl chloride, polystyrene, derivatized cellulose), plasticizers in polymer (to improve permeability and hence response) [5] have been used as common supports. Another versatile anchoring scheme uses sol-gel inclusion [6]. Sol-gel techniques that use covalent bonding for dye entrapment have been

* Corresponding author.

E-mail address: dutta.1@osu.edu (P.K. Dutta).

reported, with reduced dye loss but the luminescent properties are somewhat compromised [6c]. Typical problems in design of optical sensors involve the insolubility of the dyes in the hydrophobic support matrices, leaching and photodecomposition of the sensitizer.

Zeolites, with their novel cage structure also provide an alternative support. For example, zeolite Y consists of 13 Å supercages with 7 Å windows, ensuring that a sensitizer like tris(bipyridyl) ruthenium (II), $\text{Ru}(\text{bpy})_3^{2+}$, with a diameter of 12 Å is securely entrapped, thus preventing leaching of the dye [7]. Oxygen is an efficient quencher of photoexcited $\text{Ru}(\text{bpy})_3^{2+}$ by an energy transfer process, and the resulting deactivation of $\text{Ru}(\text{bpy})_3^{2+*}$ allows for spectroscopic monitoring by emission intensity [8].

Meier et al. [9] have exploited this encapsulation technique for making optical oxygen sensors. They used dealuminated zeolite Y with Si/Al ratio of 6 and quenching was reported upon exposure to gas phase O_2 , and advantages of using zeolites as host was well documented. Fig. 1 plots the change in luminescence intensity of $\text{Ru}(\text{bpy})_3^{2+}$ in zeolites Y of Si/Al ratios of 2.5 and 6.5 (dispersed in polydimethylsiloxane (PDMS) films) upon exposure to N_2 and O_2 dissolved in water. It is clear that both zeolite-based samples do quite poorly when

measuring dissolved O_2 and the fact is that in our hands we could reproduce the data in Ref. [9] with partially dealuminated (Si/Al = 6.5) zeolites for gas phase O_2 , but the response to dissolved O_2 was poor, as shown in Fig. 1. For comparison, the change in luminescence is also shown for an aqueous solution of $\text{Ru}(\text{bpy})_3^{2+}$ in Fig. 1. The relative quenching efficiencies (QE) defined as $((I_{\text{N}_2} - I_{\text{O}_2}) / I_{\text{N}_2} \times 100)$ were 0%, 2%, and 66% for zeolite Y (Si/Al = 2.5), (Si/Al = 6.5) and aqueous $\text{Ru}(\text{bpy})_3^{2+}$, respectively, where I is the luminescence intensity of $\text{Ru}(\text{bpy})_3^{2+}$ measured at 607 nm (450 nm excitation). The data in Fig. 1 suggests that the accessibility of the entrapped $\text{Ru}(\text{bpy})_3^{2+}$ inside the zeolite to O_2 is hindered, and in a recent study, we have determined that this is primarily due to intrazeolitic water, which impedes the diffusion of O_2 through the zeolite [10]. Thus, it is not surprising that we do not detect dissolved oxygen in water using the aluminous zeolites, since water blocks the diffusion of O_2 .

In this study, we report that the use of highly siliceous (Si/Al > 100) zeolites alleviates the problems of intrazeolitic O_2 diffusion, and propose a sensor design for dissolved oxygen. The use of highly siliceous zeolites required the development of alternative synthesis procedures for entrapment of $\text{Ru}(\text{bpy})_3^{2+}$. Transport of O_2 from water to the zeolite has been examined. PDMS films with the siliceous zeolites were fabricated and the quenching of $\text{Ru}(\text{bpy})_3^{2+*}$ with dissolved oxygen was tested. The photochemical stability of the sensors was studied.

2. Experimental section

2.1. Materials

Zeolite-Y (Si/Al = 2.5) used in this study was purchased from Union Carbide and cleaned by ion-exchange and calcination. Hexaammine ruthenium chloride (III), ruthenium (III) chloride, anhydrous (48.45% Ru) and SiCl_4 were obtained from Strem Chemicals and Aldrich. N_2 (99.99%), O_2 (99.99%), N_2/O_2 (60/40) were purchased from Praxair. The PDMS (RTV 615A and 615B) was obtained from GE Silicones.

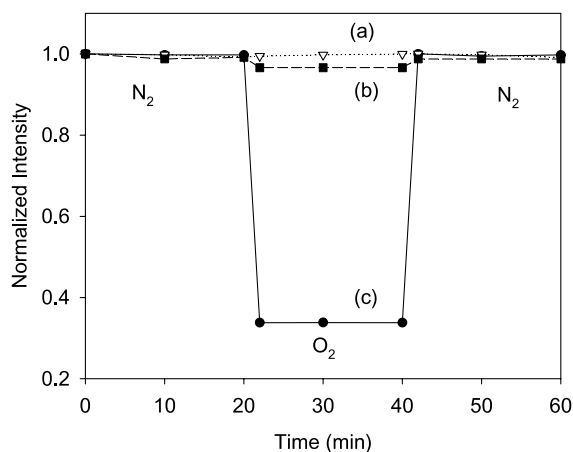


Fig. 1. Quenching profile as measured by the intensity of the 607 nm band for PDMS membranes containing (a) zeolite Y– $\text{Ru}(\text{bpy})_3^{2+}$ (Si/Al = 2.5), (b) zeolite Y– $\text{Ru}(\text{bpy})_3^{2+}$ (Si/Al = 6.5) and (c) 1×10^{-5} M $\text{Ru}(\text{bpy})_3^{2+}$ in water.

2.2. Dealumination of Zeolite Y

Literature procedures were followed to generate siliceous zeolites [11]. A fixed bed vertical reactor made entirely of quartz was used for dealumination. Zeolite powder was supported on a quartz holder, and the temperature of reaction was measured with a thermocouple inserted into the zeolite bed. Prior to dealumination, 1 g of zeolite was dehydrated in situ at 400 °C under flowing dry nitrogen. The temperature was then lowered to ≈ 200 °C and a nitrogen stream saturated with SiCl_4 was brought into contact with zeolite. The sample was treated with SiCl_4 vapor for 4 h, followed by purging with dry nitrogen. The zeolite was cooled, washed with distilled water (checked for chloride), and dried at 80 °C in a vacuum oven.

Acid leaching and steam treatment: After SiCl_4 treatment, the dry sample was stirred with 3.8 M HCl at 90 °C for 3 h. The sample was then centrifuged and washed several times with distilled water. After acid leaching, the zeolite was put in a reactor and heated to 700 °C and steam was passed through the sample for 16 h, followed by N_2 .

2.3. $\text{Ru}(\text{bpy})_3^{2+}$ -Zeolite Y ($\text{Si}/\text{Al}=2.5$)

The divalent ruthenium complex was synthesized by previously reported procedures [12]. The loading levels were kept at ~ 1 $\text{Ru}(\text{bpy})_3^{2+}$ per 15 supercages.

2.4. Synthesis of $\text{Ru}(\text{bpy})\text{Cl}_3$ [13]

RuCl_3 (0.064 g, 0.308 mmol), LiCl (0.030 g, 0.709 mmol), and 2,2'-bipyridyl (0.048 g, 0.308 mmol) were taken in a round bottom flask, and 25 ml DMF was added and stirred for 8 h at 90 °C. $\text{Ru}(\text{bpy})\text{Cl}_3$ was purified from the brownish solution by two different procedures. (i) Diethyl ether was added into the DMF reaction mixture, and kept in the refrigerator for about 3 h. The solvent mixture was decanted and the brown-red oily compound was dissolved in CH_3CN . The solution was filtered to remove LiCl and used for reaction with zeolite. (ii) $\text{Ru}(\text{bpy})\text{Cl}_3$ was separated by column chromatography using silica gel and CH_3CN or

DMF as eluent. TLC showed major product is $\text{Ru}(\text{bpy})\text{Cl}_3$.

2.5. $\text{Ru}(\text{bpy})_3^{2+}$ -dealuminated Y

Siliceous zeolite was activated at 500 °C under vacuum, and added to the red CH_3CN solution of $\text{Ru}(\text{bpy})\text{Cl}_3$ and stirred in N_2 at room temperature for 40 h and centrifuged and washed with CH_3CN . The solid sample was dispersed in 50 ml of ethanol. Excess 2,2'-bipyridyl (0.338 g, 2.2 mmol) was added and refluxed for 3 days. The orange colored solid was washed several times with ethanol and CH_3CN . The excess ligand was Soxhlet-extracted with ethanol until bipyridine was no longer present, as measured by UV-visible spectroscopy.

2.6. PDMS-zeolite membrane

Siliceous $\text{Ru}(\text{bpy})_3^{2+}$ zeolite was dehydrated at 100 °C under vacuum for 12 h and 30 mg added to 650 mg of cyclohexane and sonicated for 4 h. Five hundred mg of RTV 615A was mixed with 60 mg of the cyclohexane treated zeolite and 500 mg of dry hexane and sonicated for 5 h. Then 60 mg of RTV 615B was added, and the mixture was sonicated for an additional 30 min. The mixture was cast onto a glass plate and kept in a vacuum oven at 60 °C overnight. Typical film thickness ranged from 20 to 30 μm .

2.7. Luminescence spectroscopy

Emission measurements were done using a SPEX Fluorolog fluorimeter. For Stern-Volmer analysis, experiments were done with water saturated with nitrogen (99.99%), air, oxygen (99.99%) or a 60/40 mixture of oxygen/nitrogen.

2.8. Zeolite characterization

X-ray powder diffraction spectroscopy was performed with Rigaku Geigerflex diffractometer using Ni-filtered $\text{CuK}\alpha$ radiation (40 kV and 25 mA). IR spectra were recorded with Perkin Elmer fourier transform IR spectrometer. Solid-state ^{29}Si NMR were obtained with a Bruker AM 500 NMR spectrometer. Ru analysis was done with ICP-OES.

3. Results

3.1. Synthesis and characterization of $Ru(bpy)_3^{2+}$ -siliceous zeolite Y

Highly siliceous zeolites were made by dealumination of zeolite Y (Si/Al=2.5) with $SiCl_4$ by procedures described in the literature [11]. Acid leaching and steaming were done to remove entrapped aluminate species, hydroxyl nests and incorporate amorphous silica. The powder diffraction pattern of the siliceous zeolite is shown in Fig. 2. The crystallinity of the sample is preserved. The ^{29}Si NMR spectra before and after acid leaching and steam treatment are shown in Fig. 3. The steam treated samples show only a single, sharp peak at -107.5 ppm due to $Si(OSi)_4$ sites with no evidence of amorphous silica or Si-OH groups in the final sample [11c]. The IR spectra exhibited the typical changes that are expected after dealumination, bands at 457, 506, 578, 720 and 789 are shifted to 461, 531, 610, 788 and 836 cm^{-1} upon $SiCl_4$ treatment [11a]. Based on the literature [11] and our spectroscopic data, we estimate that the Si/Al ratio of the framework is >100 , and henceforth use the notation Si-Y to indicate this material.

There have been many studies on synthesis of $Ru(bpy)_3^{2+}$ within zeolite Y using “ship-in-a-bottle” strategies, which all start with ion-exchange of the zeolite with $Ru(NH_3)_6^{3+/2+}$ species [12,14]. Unfortunately, in Si-Y, there are no ion-exchangeable sites

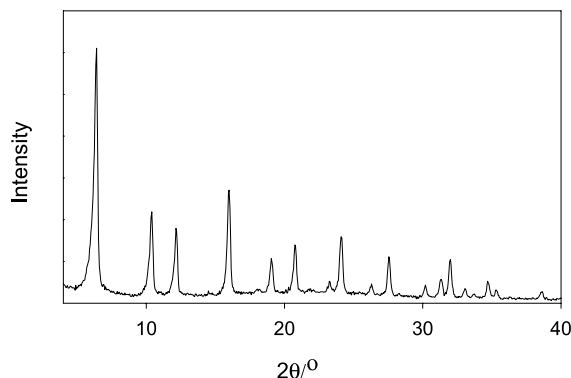


Fig. 2. Powder diffraction pattern of siliceous zeolite after acid treatment and steaming.

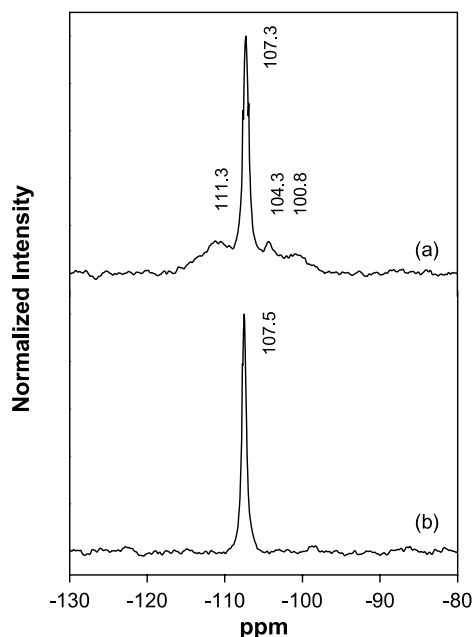
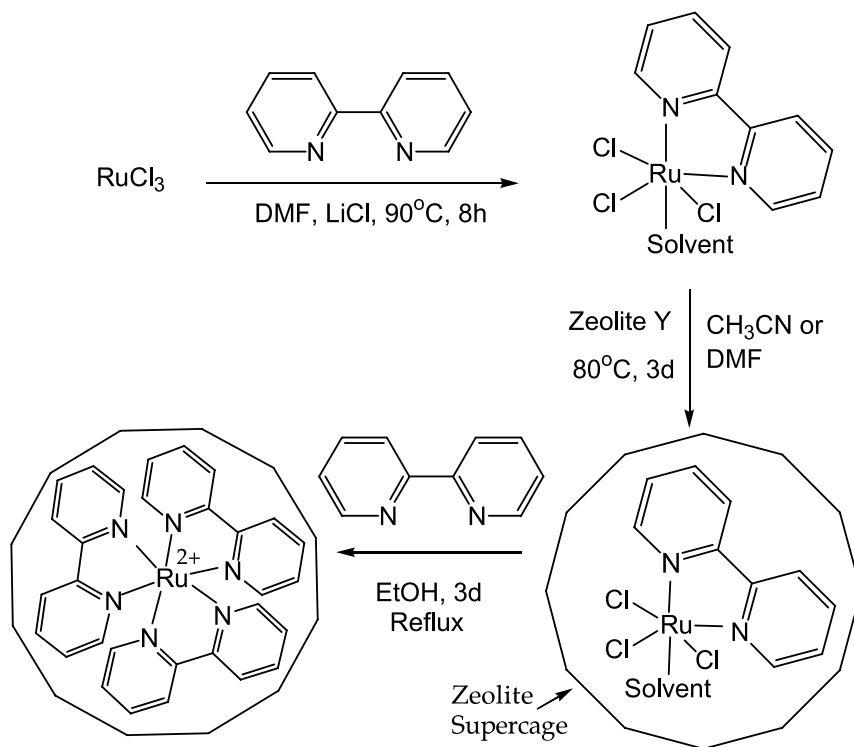


Fig. 3. ^{29}Si NMR spectra of (a) siliceous zeolite and (b) after acid treatment and steaming.

because of the lack of Al, and the conventional procedure cannot be used. An option is to synthesize $Ru(bpy)_3^{2+}$ -zeolite Y (Si/Al=2.5) and then dealuminate the sample. Considering that it is unlikely that $Ru(bpy)_3^{2+}$ would survive the harsh conditions present during dealumination reactions, this was not attempted. This led us to the synthesis procedure shown in Scheme 1, where the solubility of $Ru(bpy)Cl_3$ in organic solvents was exploited to introduce ruthenium into the siliceous zeolite. However, this adsorption method of loading led to low levels of Ru incorporation, about 1 per 10 000 supercages, as compared to methods that use ion-exchange for aluminous zeolites, where a maximum of 1 $Ru(bpy)_3^{2+}$ per 2 supercages can be synthesized [15].

Fig. 4a shows the diffuse reflectance spectrum of $Ru(bpy)_3^{2+}$ -Si-Y and is characterized by bpy ligand transitions at 286 nm and the metal-to-ligand charge transfer band at 450 nm. Upon excitation of the sample at 450 nm, the emission spectrum shown in Fig. 4b was observed, with the peak at 607 nm. These spectra are in agreement with those reported for $Ru(bpy)_3^{2+}$ in aluminous zeolites [7,12,14,15].



Scheme 1. Synthesis of Ru(bpy)₃²⁺ in highly hydrophobic zeolite Y using Ru(bpy)Cl₃.

3.2. O₂ transport from water to intrazeolitic space

The emission spectrum of the surface of a Ru(bpy)₃²⁺-Si-Y pellet immersed in water was monitored as the solution was altered between N₂ and O₂-saturated water. The intensity of the band at 607 nm (normalized to the N₂ value) was measured as a function of time and shown in Fig. 5a. In O₂-saturated water, the quenching was of the order of 23% and upon changing to N₂-saturated water, the intensity recovered.

Pellets of Ru(bpy)₃²⁺-Si-Y were exposed to cyclohexane and benzene. These pellets were then immersed in N₂- and O₂-saturated water and the emission spectra were measured. The emission data are shown in Fig. 5b and c. Upon exposure to O₂-saturated water, the order of quenching was benzene > cyclohexane, with quenching efficiencies of ~32% and 35%, respectively. The solubility of cyclohexane and benzene in water is 0.008 and 0.18 g/ml, respectively [16]. Considering the hy-

drophobic nature of the siliceous zeolite [17], and low aqueous solubilities of the solvents, it is not expected that there will be loss of solvent from the zeolite upon exposure to water.

3.3. Dissolved oxygen sensing

For use of Ru(bpy)₃²⁺-Si-Y as a dissolved oxygen sensor, the zeolite crystallites were dispersed into PDMS films. Fig. 6 shows an optical micrograph of such a film (magnification 14×). For comparison, we also show a PDMS film made with Ru(bpy)₃²⁺-zeolite Y of Si/Al = 2.5 (loading level-1 Ru(bpy)₃²⁺ per 15 supercages). The difference in overall color of the films arises from the lower loading of Ru(bpy)₃²⁺ in the siliceous zeolite. The aluminous zeolites (crystallite size 1 μm) tend to cluster into 100–300 μm aggregates, whereas dealuminated zeolites make clearer films with uniform distribution of the crystallites, as evidenced by the uniformity of color, as well as better opacity. This

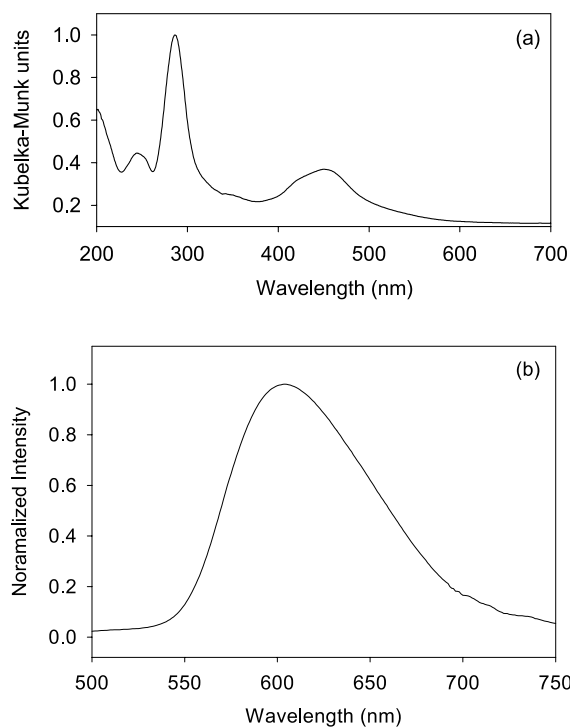


Fig. 4. (a) Diffuse reflectance and (b) emission spectra of $\text{Ru}(\text{bpy})_3^{2+}\text{-Si-Y}$ (excitation-450 nm).

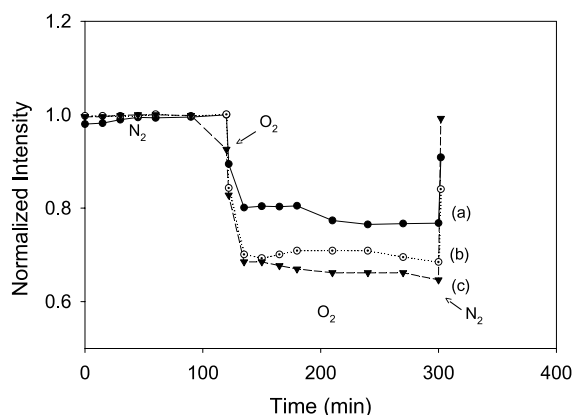


Fig. 5. Quenching profile as measured by the intensity of the 607 nm band for pellets of $\text{Ru}(\text{bpy})_3^{2+}\text{-Si-Y}$ exposed to O_2/N_2 dissolved in water (a) pellet alone, (b) cyclohexane saturated pellet, (c) benzene saturated pellet (at each point, the emission spectra were collected over 500–700 nm range with 450 nm excitation, ~0–100 min N_2 , ~100–300 min O_2 , >300 min N_2).

could arise from the highly hydrophobic nature of Si-Y crystallites making dispersion in the PDMS

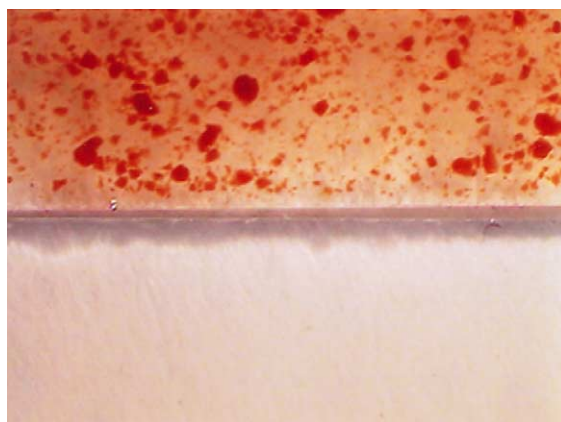


Fig. 6. Optical micrographs of PDMS films with $\text{Ru}(\text{bpy})_3^{2+}\text{-zeolite Y}$ ($\text{Si/Al}=2.5$) (above) and $\text{Ru}(\text{bpy})_3^{2+}\text{-Si-Y}$ (below). Magnification was 14 \times (particles in zeolite Y were agglomerates of 100–300 μm).

favorable. The better optical properties are possibly a result of the closer match of the refractive index of the siliceous zeolite and the polymer matrix.

Fig. 7 shows the change in normalized emission intensity upon exposure of a $\text{Ru}(\text{bpy})_3^{2+}\text{-Si-Y}$ PDMS film (referred to henceforth as Ru-Y-PDMS film) on glass to N_2 , O_2 and mixtures of N_2 and O_2 all as dry gases. Fig. 8 shows the data for the Ru-Y-PDMS film immersed in solution of N_2 - and O_2 -saturated water. In the case of dry O_2 , the quenching of the $\text{Ru}(\text{bpy})_3^{2+}\text{-Si-Y}^*$ emission is of the order of 63%, whereas for O_2 -saturated water, the quenching is 55%. Response times cannot be evaluated from these data, since at each point, the emission spectrum was obtained between 500 and 700 nm (which typically requires a few minutes).

Fig. 9 compares the Stern-Volmer plots for the Ru-Y-PDMS films for dry gas streams and aqueous dissolved gas streams. Both curves are nonlinear with a diversion in the curves at the higher O_2 concentrations, with more quenching in the gas phase. Fig. 10 shows the long-term stability of a film as measured by the quenching efficiency in N_2 versus O_2 -saturated water as a function of illumination time. The mean value of quenching was 55% with a standard deviation of 5%.

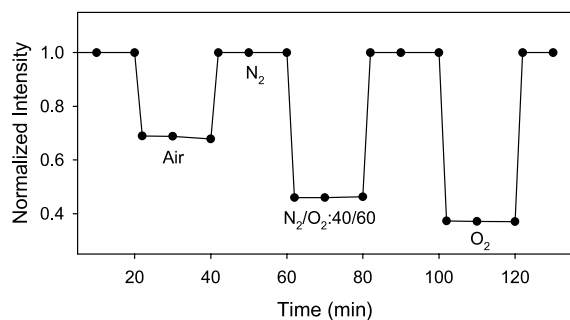


Fig. 7. Quenching profile of $\text{Ru}(\text{bpy})_3^{2+}$ -Si-Y in PDMS membrane exposed to dry gases (at each point, the emission spectra were collected over 500–700 nm range with 450 nm excitation, and the intensity monitored at 607 nm).

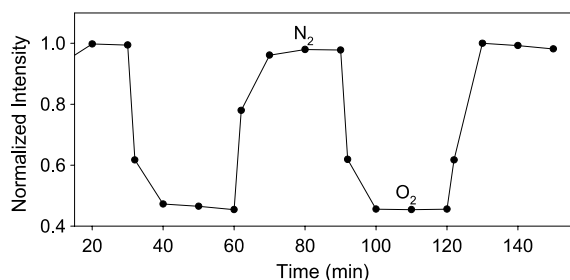


Fig. 8. Quenching profile of $\text{Ru}(\text{bpy})_3^{2+}$ -Si-Y in PDMS membrane exposed to gases dissolved in water (at each point, the emission spectra were collected over 500–700 nm range with 450 nm excitation, and the intensity monitored at 607 nm).

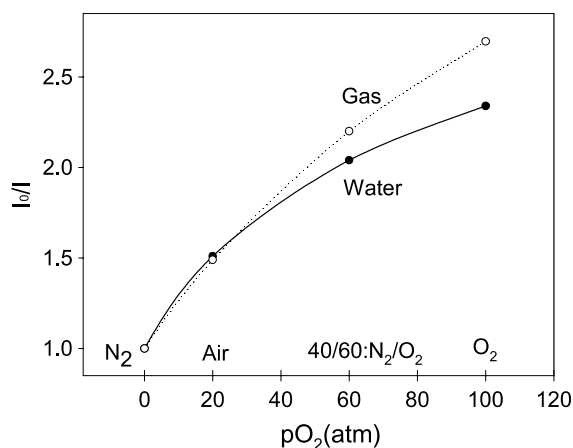


Fig. 9. Stern-Volmer plot of $\text{Ru}(\text{bpy})_3^{2+}$ -Si-Y in PDMS membrane exposed to dissolved gases.

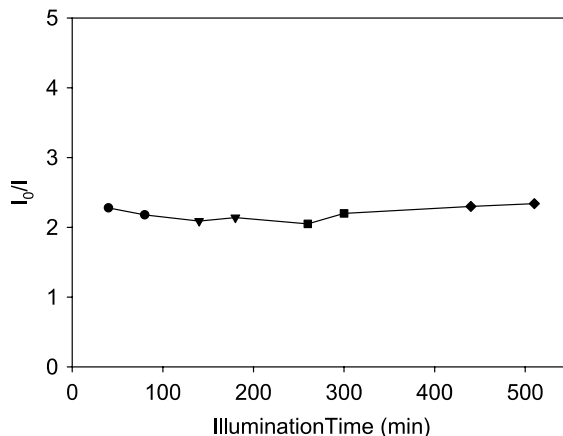


Fig. 10. Dependence of quenching for a $\text{Ru}(\text{bpy})_3^{2+}$ -Si-Y in PDMS membrane exposed to O_2/N_2 dissolved in water with illumination time.

4. Discussion

The goal of this program was to encapsulate the dye molecule $\text{Ru}(\text{bpy})_3^{2+}$ in the supercages of zeolite Y and use the luminescence quenching of photoexcited $\text{Ru}(\text{bpy})_3^{2+}$ by O_2 as a measure of oxygen dissolved in water. However, as shown in Fig. 1, transport of O_2 from water into zeolites with low Si/Al ratios was poor and so was the quenching efficiency. We have reported earlier that the lack of O_2 penetration is because of the diffusional restriction due to intrazeolitic water molecules [10]. A study with highly siliceous zeolites was undertaken because it is well known that such zeolites tend to be hydrophobic and repel water [17].

Comparison of $\text{Ru}(\text{bpy})_3^{2+}$ -PDMS films made with aluminous zeolites (Fig. 1a and b) with siliceous zeolites (Fig. 8) shows that dealumination makes a major difference in transport of N_2/O_2 dissolved in water to the intrazeolitic space. Considering the level of dealumination and the fact that extra steaming and thermal treatments were undertaken to remove any amorphous silica or Si-OH groups (as evidenced from the NMR data [11c], there should be no H_2O molecules within the zeolite. Thus, transport of N_2/O_2 occurs from water to the empty intracrystalline space. Previous studies of quenching of dyes in a wide range of matrices have shown that the O_2 quenching of the

excited state follows dynamic quenching [18]. Although lifetime studies of $\text{Ru}(\text{bpy})_3^{2+}$ quenching with O_2 have not yet been done with siliceous zeolites, intrazeolitic pyrene quenching by O_2 has been reported to be dynamic [19] and dynamic quenching is indeed expected for the present study.

Zeolites are well known adsorbers that exploit the differences in adsorption between N_2 and O_2 to separate these gases by a method referred to as pressure swing adsorption (PSA) [20]. The separation is achieved because N_2 with a quadrupole moment of 0.31 \AA^3 interacts more strongly with zeolitic cations than O_2 with a quadrupole moment of 0.1 \AA^3 . However, in the highly siliceous zeolites being examined in this study, there are no zeolite cations, and thus it is expected that the composition of N_2/O_2 within the zeolite should reflect well the composition of the gas (either as gas or dissolved).

It has been noted that for porous silica sol–gel films with increasing hydrophobicity, the quenching of the entrapped sensitizer by dissolved O_2 increases and has been explained as arising due to increased O_2 partitioning in the hydrophobic matrix [6b]. The extent of gas partitioning between water and the zeolite is determined by the “solubility” of gases in the zeolite. Indeed, this concept of solubility is reinforced when experiments were done with different solvents in the intrazeolitic space. The solvents chosen were cyclohexane and benzene. The quenching of the intrazeolitic $\text{Ru}(\text{bpy})_3^{2+}$ by O_2 dissolved in water increased in the order benzene > cyclohexane > empty zeolite. Without any solvent, the extent of quenching was 23%, whereas with cyclohexane and benzene in the zeolite, the quenching levels increased to 33% and 35%, respectively. Based on the Henry’s constant for O_2 at 293 K, we calculate the solubilities of O_2 in water, benzene and cyclohexane for an oxygen partial pressure of 1 atm to be ~ 40 , 288, and 371 mg/l [21]. In the case of cyclohexane and benzene, the transfer of O_2 from H_2O to the intrazeolitic space is promoted by the increased solubility of O_2 in these solvents as compared to water. However, it is to be noted that even though the solubility of O_2 in cyclohexane is greater than in benzene, the level of quenching is reversed. Besides solubility, the diffusion of O_2 within the solvent-saturated

zeolites is also of relevance and is under investigation. The hydrophobic zeolite also has higher solubility towards O_2 as compared to H_2O , but here the transport is from the aqueous medium to a “gas-phase” like environment within the zeolite.

Considering the uptake of N_2/O_2 dissolved in H_2O into the Ru–Si–Y, the possibility of using these zeolite crystals as O_2 sensors was examined. The zeolite was dispersed in PDMS films [22]. The quality of the films with the siliceous zeolites, as far as opacity and uniformity of dispersion was concerned is considerably better than the aluminous zeolites and is also attractive for fabrication of the sensor platform.

The Stern–Volmer plots obtained with the films for both gas-phase and dissolved gases were non-linear. Such nonlinearity in Stern–Volmer plots has usually been ascribed to heterogeneity in the distribution of the sensitizer [23]. In the zeolite, since it is a well-ordered crystalline structure, at low loadings of $\text{Ru}(\text{bpy})_3^{2+}$, there should be no site heterogeneity, since each molecule is in a separate supercage and separated from other molecules by neighboring empty supercages [15]. Thus, in our previous study with more aluminous zeolites, the site heterogeneity was explained as arising from structural defects within the zeolite during the synthesis of $\text{Ru}(\text{bpy})_3^{2+}$ within the zeolite [10]. Highly siliceous zeolites are hydrothermally stable, so deterioration of the crystal structure is not expected during the $\text{Ru}(\text{bpy})_3^{2+}$ synthesis. We propose that the distribution of $\text{Ru}(\text{bpy})_3^{2+}$ is possibly not homogeneous through the zeolite, unlike in the more aluminous zeolites, where the ruthenium species is introduced by ion-exchange. Even though $\text{Ru}(\text{bpy})\text{Cl}_3$ is a neutral molecule and is introduced in the zeolite via adsorption, its polarity must make it difficult to penetrate deep into the highly siliceous zeolite. We propose that there is a higher concentration of dye towards the surface of the pellet than the interior.

The higher response of the Ru–PDMS films to gas phase O_2 as compared to dissolved O_2 is consistent with studies with organically modified sol–gel silica [6b]. Since the number density of oxygen molecules in the gas phase is ~ 30 times higher than a saturated aqueous solution (9.2 ppm at 20 °C) [6b], the amount of quenching in the gas phase was higher.

From a practical point of view, there are several advantages to zeolite encapsulated dyes, as has been outlined in a previous study [9]. The long-term quenching measurements show about 5% deviation in the relative quenching efficiency over a constant illumination period of 8 h. Loss of sensitizer is only possible if the silica framework is dissolved, and will only happen in HF. Thus, dissolved O₂ measurements can be made in all organic solvents and ranging from strongly acidic to basic solutions. Also, Ru(bpy)₃²⁺-zeolite samples have been heated to ~250 °C without any apparent decomposition, so considerable thermal stability is expected [24]. We have recently reported on the photodissociation chemistry of zeolite entrapped Ru(bpy)₃²⁺ [25]. Because of the neutrality of the zeolite framework, the only possible way that ligand displacement can occur is by attack of water or chloride ions. Since there are no water molecules in hydrophobic zeolites, this route of photodissociation is eliminated. Based on the work of Hartmann and coworkers, we can discount the decomposition of Ru(bpy)₃²⁺ by attack of singlet oxygen, ¹O₂ [26]. Any photodecomposition resulting from disproportionation reactions is remote because of the low loading of the dye and their encapsulation within the supercage [27].

5. Conclusions

Highly siliceous zeolite was made by SiCl₄ treatment of a low Si/Al zeolite Y and made defect-free by acid treatment and steaming. Ru(bpy)₃²⁺ was synthesized within the supercages of the siliceous zeolite using Ru(bpy)Cl₃ as the starting material. Dealumination of the zeolite and the resulting hydrophobicity resulted in transport of O₂ dissolved in water into the zeolite and emission quenching of photoexcited Ru(bpy)₃²⁺ was readily observed. Transparent PDMS films of the zeolite were made and Stern–Volmer plots were obtained. Non-linearity in the Stern–Volmer plots was explained as arising from inhomogeneous distribution of the Ru(bpy)₃²⁺ within the zeolite, with more dye nearer the zeolite surface. The long-term stability of the Ru(bpy)₃²⁺-siliceous zeolite is expected

to be high, since there will be no dye leaching and photodecomposition is also minimized.

Acknowledgements

We acknowledge funding from NSF (EEC 9872531) and NASA.

References

- [1] (a) M.L. Hitchman, *Measurement of Dissolved Oxygen*, Wiley, New York, 1978;
(b) J.N. Demas, B.A. DeGraff, P.B. Coleman, *Analytical Chemistry News and Features* (1999) 793A.
- [2] (a) D. García-Fresnadillo, M.D. Marazuela, M.C. Moreno-Bondi, G. Orellana, *Langmuir* 15 (1999) 6451;
(b) B.D. MacCraith, C.M. McDonagh, G. O'Keefe, E.T. Keyes, J.G. Vos, B. O'Kelly, J.F. McGilp, *Analyst* 118 (1993) 385;
(c) E.R. Carraway, J.N. Demas, B.A. DeGraff, J.R. Bacon, *Journal of American Chemical Society* 63 (1991) 337;
(d) A. Mills, *Sensors and Actuators B: Chemical* 51 (1998) 60.
- [3] W. Xu, R.C. McDonough, B. Langsdorf, J.N. Demas, B.A. DeGraff, *Analytical Chemistry* 66 (1994) 4133.
- [4] (a) X. Lu, M.A. Winnik, *Chemistry of Materials* 13 (2001) 3449;
(b) P. Hartmann, M.J.P. Leiner, M.E. Lippitsch, *Analytical Chemistry* 67 (1995) 88;
(c) O.S. Wolfbeis, M.J.P. Leiner, H.E. Posch, *Mikrochimica Acta III* (1986) 359;
(d) H.N. McMurray, P. Douglas, C. Busa, M.S. Garley, *Journal of Photochemistry and Photobiology A: Chemistry* 80 (1994) 283.
- [5] A. Mills, M.D. Thomas, *Analyst* 23 (1998) 1135.
- [6] (a) C.M. McDonagh, A.M. Shields, A.K. McEvoy, B.D. MacCraith, J.F. Gouin, *Journal of Sol–Gel Science and Technology* 13 (1998) 207;
(b) C. McDonagh, B.D. MacCraith, A.K. McEvoy, *Analytical Chemistry* 70 (1998) 45;
(c) A. Lobnik, I. Oehme, I. Murkovic, O.S. Wolfbeis, *Analytica Chimica Acta* 367 (1998) 159.
- [7] A.S. Vaidyalangam, M.A. Coutant, P.K. Dutta, in: V. Balzani (Ed.), *Electron Transfer in Chemistry*, Wiley-VCH, 2001, p. 412.
- [8] J.N. Demas, E.W. Harris, R.P. McBride, *Journal of American Chemical Society* 99 (1977) 3547.
- [9] B. Meier, T. Werner, I. Klimant, O.S. Wolfbeis, *Sensors and Actuators B: Chemical* 29 (1995) 240.
- [10] M.A. Coutant, P. Payra, P.K. Dutta, *Microporous and Mesoporous Materials* 60 (2003) 79.
- [11] (a) M.W. Anderson, J.J. Klinowski, *Journal of the Chemical Society, Faraday Transactions 1* (8) (1986) 1449;

- (b) H.K. Beyer, I.M. Belenykaja, F.J. Hange, *Journal of the Chemical Society, Faraday Transactions 1* (81) (1985) 2889;
(c) G.J. Ray, A.G. Nerheim, J.A. Donohue, *Zeolites* 8 (1988) 458.
- [12] (a) W. DeWilde, G. Peeters, J.H. Lunsford, *Journal of Physical Chemistry* 84 (1980) 2306;
(b) K. Maruszewski, D.P. Strommen, J.R. Kincaid, *Journal of American Chemical Society* 115 (1993) 8345;
(c) M.A. Coutant, T. Le, N.B. Castagnola, P.K. Dutta, *Journal of Physical Chemistry B* 104 (2000) 10783.
- [13] D. Hesk, Y. Inoue, S.R.L. Everitt, H. Ishida, M. Kunieda, M.G.B. Drew, *Inorganic Chemistry* 39 (2000) 308.
- [14] N.B. Castagnola, P.K. Dutta, *Journal of Physical Chemistry B* 102 (1998) 1696.
- [15] (a) P. Laine, M. Lanz, G. Calzaferri, *Inorganic Chemistry* 35 (1996) 3514;
(b) M. Sykora, J.R. Kincaid, P.K. Dutta, N.B. Castagnola, *Journal of Physical Chemistry B* 103 (1999) 309.
- [16] R. Battino (Ed.), *Hydrocarbons with water and seawater Part 1: Hydrocarbons C₅ to C₇, Solubility Data Series, Volume 37*, Pergamon Press, New York, 1989.
- [17] (a) H. Yang, Z. Ping, G. Niu, H. Jiang, Y. Long, *Langmuir* 15 (1999) 5382;
(b) C.K.W. Meininghaus, R. Prins, *Microporous and Mesoporous Materials* 36 (2000) 349.
- [18] E.R. Carraway, J.N. Demas, *Langmuir* 7 (1991) 2991.
- [19] X. Liu, K.-K. Iu, J.K. Thomas, *Journal of Physical Chemistry* 93 (1989) 4120.
- [20] R.V. Jasra, N.V. Choudary, S.G.T. Bhat, *Separation Science and Technology* 26 (1991) 885.
- [21] (a) E. Wilhelm, R. Battino, *Chemical Reviews* 73 (1973) 1;
(b) P. Lühring, A. Schumpe, *Journal of Chemical and Engineering Data* 34 (1989) 250;
(c) T.R. Rettich, R. Battino, E. Wilhelm, *Journal of Chemical Thermodynamics* 32 (2000) 1145.
- [22] (a) I.F.J. Vankelecom, E. Scheppers, R. Heus, J.B. Uytterhoven, *Journal of Physical Chemistry* 98 (1994) 12390;
(b) M.-D. Jia, K.-V. Peinemann, R.-D. Behling, *Journal of Membrane Science* 73 (1992) 119;
(c) I.F.J. Vankelcom, C. Dotremont, M. Morobé, J.-B. Uytterhoeven, C. Vandecasteele, *Journal of Physical Chemistry B* 101 (1977) 2154.
- [23] E.R. Carraway, J.N. Demas, B.A. DeGraff, J.R. Bacon, *Analytical Chemistry* 63 (1991) 337.
- [24] J.A. Incavo, P.K. Dutta, *Journal of Physical Chemistry* 94 (1990) 3075.
- [25] A. Vaidyalngam, P.K. Dutta, *Analytical Chemistry* 72 (2000) 5219.
- [26] P. Hartmann, *Analytical Chemistry* 72 (2000) 2828.
- [27] B.H. Milosavijevic, J.K. Thomas, *Journal of Physical Chemistry* 87 (1983) 616.